12.479 Trace-Element Geochemistry
Spring 2009

Lecture 6

A. Determination of Partition Coefficients:

There are two approaches for determination of partition coefficients: (1) analyses of coexisting phases in natural rocks or (2) analyses of phases in experimental systems when parameters such as pressure and temperature are controlled.

Analyses of natural rocks, typically involves

(1) Phenocryst/matrix partitioning: In this case the phenocrysts are assumed to represent minerals that formed in equilibrium with a melt that is now represented by a glass or a fine-grained matrix; therefore mineral/melt partition coefficients can be inferred.

(2) Mineral/mineral partitioning: for example, in metamorphic rocks, such as upper mantle peridotites, the coexisting phases can be analyzed.

B. Discussion of Phenocryst/matrix Approach:

In this lecture we focus on the early studies of natural rocks which served to establish the first order systematics of trace element partitioning. Before we look at typical results, it is important to discuss the advantages and limitations of this approach, i.e., inferring D values from analyses of phenocryst/matrix pairs.

(1) Advantages: the principal advantage is that if the objective is determining the petrogenesis of a specific group of igneous rocks, the appropriate partition coefficients are inferred from the rocks being studied; in particular, the pressure, temperature and melt composition are directly applicable to the rocks being studied. In contrast, experimental determination of partition coefficients are commonly done at a single pressure in a compositionally simple system..

(2) Problems:

(a) Each sample in a natural system has formed at a unique pressure, temperature and phase composition. The effects of these parameters in determining partition coefficients are integrated; it is not possible to infer independently the specific effects of P-T-X.

(b) Early studies required physical separation, e.g. of phenocryst and matrix. This process may be difficult and the effects of impurities, such as mineral and melt inclusions may be significant. For an incompatible element, it is particularly important to avoid any glass or groundmass contamination in the mineral separate; i.e., small amounts of contamination by a phase that is highly enriched in an incompatible element will lead to erroneous estimates of mineral/melt partition coefficients. With the advent of in situ analytical techniques such as secondary ion mass-spectrometry (SIMS or Ion-microprobe) and laser ablation inductively coupled mass spectrometry (LA-ICP-MS), it is now possible to analyze small areas (few microns) and thus avoid contaminants.

(c) Volcanic rocks often show disequilibrium textures; e.g. optical zoning of minerals in thin section reflecting compositional zonation of major elements. If major elements are zoned, one can assume that trace elements are also zoned. In this case the apparent mineral/melt partition coefficient D_{APP} can be expressed as

$$D_{APP} = \frac{\overline{C}_s}{C\ell} = \frac{1 - F^D}{(1-F)F^{(D-1)}}$$

Where $\overline{C}_S$ is the average concentration in the mineral phase; C_l is matrix composition (assumed to represent the melt), F is melt fraction and D is "real" partition coefficient.

(d) Post-magmatic alteration, in particular, the composition of a glassy or fine-grained matrix is commonly affected by post-magmatic interaction with fluids, including meteoric water.

(e) The phenocrysts may be xenocrysts. This scenario can be evaluated by observation of textures such as resorbed phase boundaries; use of major element K_D such as ~0.3 for $(Fe/Mg)_{ol}/(Fe/Mg)_{melt}$ and measurement of isotopic ratios in the two phases.

C. Phenocryst/Matrix Data: Examples

Early examples of phenocryst/matrix data are studies of partitioning of transition metals between olivine or clinopyroxene and a basaltic matrix. Two independent studies of the partitioning of first series transition metals between olivine phenocrysts and basaltic matrix (Figure 11); for every sample (1 to 13): $D_{Ni} > D_{Co} > D_{Fe} > D_{Mn}$. However, there is a significant range in absolute value, e.g., a factor of 2 for Ni, but the same range is observed in both studies

	L&S (1977)	**D&H (1972)**
Ni	13.1 to 23.5	8.6 to 18.5
Co	2.7 to 4.2	2.7 to 4.4
Sc	0.14 to 0.22	0.13 to 0.22
Cr	1.1 to 3.1	
Mn	0.7 to 1.7	1 to 1.8

Ion	Sc^{+3}	Cr^{+3}	Mn^{+2}	Fe^{+2}	Co^{+2}	Ni
Ionic Radius (VI)	0.83	0.70	0.91	0.86	0.83	0.77
Sample Origin	Olivine/matrix ratio ($D^{ol/melt}$)					
1. Solomon Islands	0.17	-	1.75	3.00	4.44	18.54
2. Western Greenland	0.13	-	1.33	1.74	2.75	8.84
3. Western Iceland	0.15	-	1.48	2.79	3.83	9.17
4. Zubair, Red Sea	0.17	-	1.28	2.28	3.66	8.63
5. Hawaii (C71)	0.22	-	1.30	1.84	4.26	11.73
6. Hawaii (C129)	0.15	-	1.04	1.75	3.62	10.67
7. Hawaii (C209)	0.18	-	1.01	1.74	4.41	14.05
8. Hawaii (KI5)	0.15	2.92	0.94	1.34	3.49	17.0
9. Hawaii (KI36)	0.15	1.23	0.83	1.53	3.24	14.8
10. Hawaii (KI44)	0.14	2.70	1.00	1.34	3.24	14.9
11. Hawaii (ML82)	0.14	1.65	1.4	1.87	4.4	21.7
12. Snake River Plain	0.22	3.06	1.67	1.80	4.19	14.4
13. Lunar Crater	0.18	1.06	0.73	1.27	2.75	8.25
Sample Number	Clinopyroxene/matrix ratio					
1	2.76	4.72	0.98	1.04	1.22	2.11
3	3.18	8.56	1.31	0.84	0.96	1.67
4	2.42	6.27	0.77	0.82	1.04	1.42
5	2.64	4.80	0.73	0.62	0.89	1.93
6	2.38	7.19	0.67	0.57	0.68	1.93
7	3.23	11.43	0.55	0.63	0.86	1.81

Notes: samples 1 through 7 from Dale and Henderson, 1972;
samples 8 through 13 from Leeman and Scheidegger (1977)

Figure 11. Partitioning of First Series Transition Metals between olivine, clinopyroxene and basaltic groundmass

A question to consider is why do D_{Co} and D_{Sc} for olivine differ (Co compatible, D = 2.7-4.2 but Sc is incompatible, D~0.2) when they have the same ionic radius? In contrast, D_{Sc} is greater than D_{Co} for clinopyroxene (Figure 11). To answer this question consider two simple formulas: forsterite (Mg_2SiO_4) and clinopyroxene as diopside ($CaMgSi_2O_6$) and investigate the possibility of Al^{+3} substituting into these two minerals to charge balance for Sc^{+3}. Al_2O_3 occurs at levels of several wt. percent in clinopyroxenes, typically >1%, but at very low levels in olivine. Apparently, the coupled substitution $Sc^{+3}Al^{+3}$ for $Mg^{+2}Si^{+4}$ is energetically favorable in clinopyroxene but not olivine. In clinopyroxene there is also the possibility of Na^{+1} substituting for Ca^{+2} as well as Al^{+3} for Si^{+4} as a charge compensation mechanism; Na_2O is commonly at levels of >0.2 wt.% in clinopyroxene.

In summary, these results show that transition metal partitioning into olivine and clinopyroxene is systematic in a relative sense. Most importantly Ni is a sensitive indicator for olivine and Sc for clinopyroxene.

D. Use of Crystal Chemistry and Ionic Model in Predicting Clinopyroxene/melt Partition Coefficients

The crystallographic structure of pyroxene consists of alternating tetrahedral and octahedral layers (Figure 12). Consider the generic formula XYZ_2O_6 for clinopyroxene: Z represents Si^{+4} and Al^{+3} in tetrahedral site, Y represents Fe^{+2}, Mg^{+2}, Al^{+3}, Cr^{+3}, and Fe^{+3} in the octahedral site, M1, and X represents the larger cations Na^{+2} and Ca^{+2} in a distorted octahedral site, M2, with CN = 8 (Figure 12).

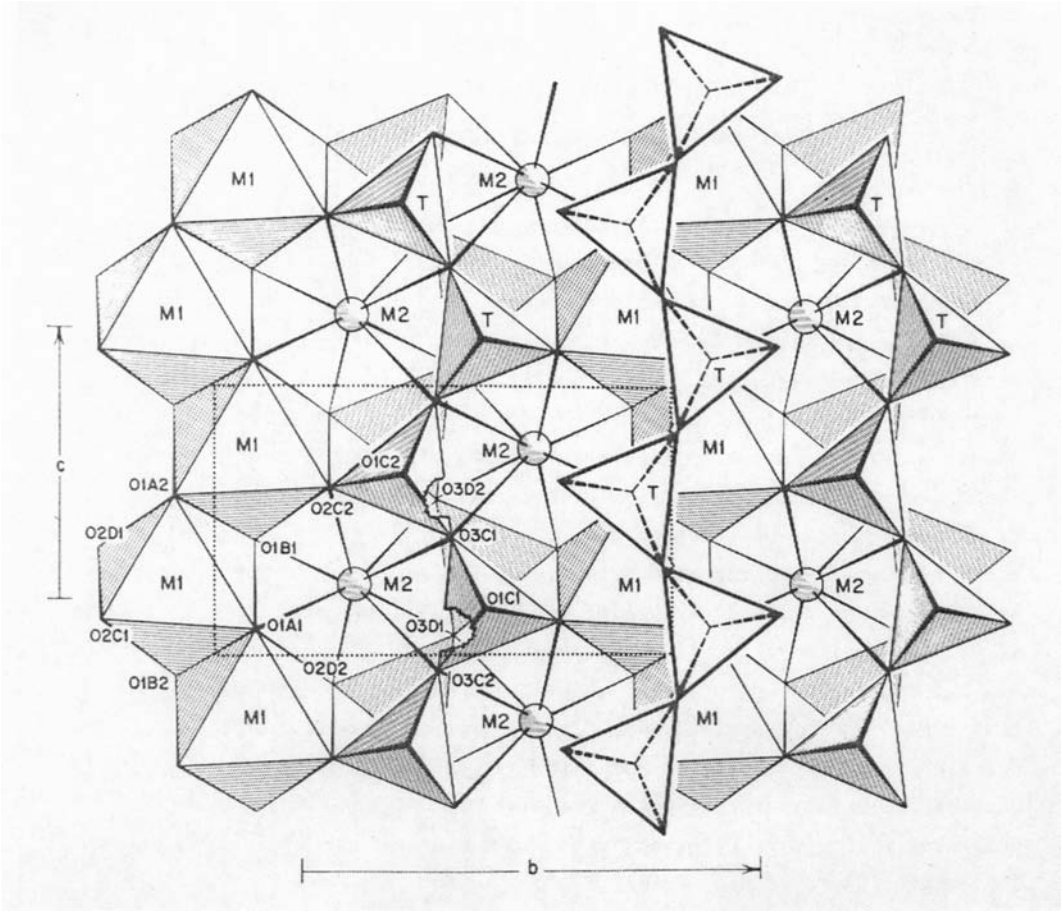

Figure courtesy of AMS.

Figure 12. Crystal structure of clinopyroxene showing chains of tetrahedra (T) connected by cations in M1 (CN=6) and M2 (CN=8) sites. Figure adapted from Cameron and Papike (1980)

Now let's consider partitioning of trace elements into clinopyroxene. The upper half of Figure 13 shows the range, and average for the six M1-O distances in clinopyroxenes of different major element composition; specifically, in their proportion of Mg/Fe/Al (i.e., diopside to acmite). Using the thick vertical line (the average M1-O distance) and subtracting 1.32A˚ as the ionic radius of O^{-2} we can estimate the "site radius", i.e. the size of the structural M1 site; it ranges from 0.7 to 0.8 A˚. We assume that trace elements

with ionic radii closest to the "site radius" will most readily be incorporated into the clinopyroxene structure; consequently, we compare the "site radius" to the ionic radii of various elements, separated into groups with the same oxidation state (lower half of Figure 13). Using only an ionic model one can predict that among +4 ions, Ti has the most favorable size, Zr is slightly too large, V slightly too small and Si is definitely too small; for +3 ions, Cr, V, Fe and Ti have appropriate sizes but Sc is slightly too large and the REE (Lu to La) are definitely too large. This prediction is in agreement with the observed $D_{Cr}^{cpx/melt}$ of 4.7 to 11.4 (Figure 11). For +2 ions Ni has an ionic radius close to the "site radius" and the mismatch between "site radius" and ionic radius increases from Ni to Co to Fe to Mn; this is exactly the order of decreasing $D_{cpx/melt}$ measured for clinopyroxene phenocrysts (Figure 11). Among the +1 ions, Li+ has a much more suitable ionic radius than Na^{+1}.

A similar comparison can be made for the M_2 site of cpx (Figure 13b), except that M_2-O distances are more variable and the bold vertical line is the average of 8 M_2-O distances and the vertical dashed line is the average of the closest six. The comparison shows that for +3 ions, intermediate atomic numbers REE are most favorable, e.g. the ionic radius of Nd is closest to average of 8 M_2-O distances; Ca is the most favorable size among +2 ions and Na among +1 ions.

E. Phenocryst/matrix partition coefficients for REE

1. Clinopyroxene

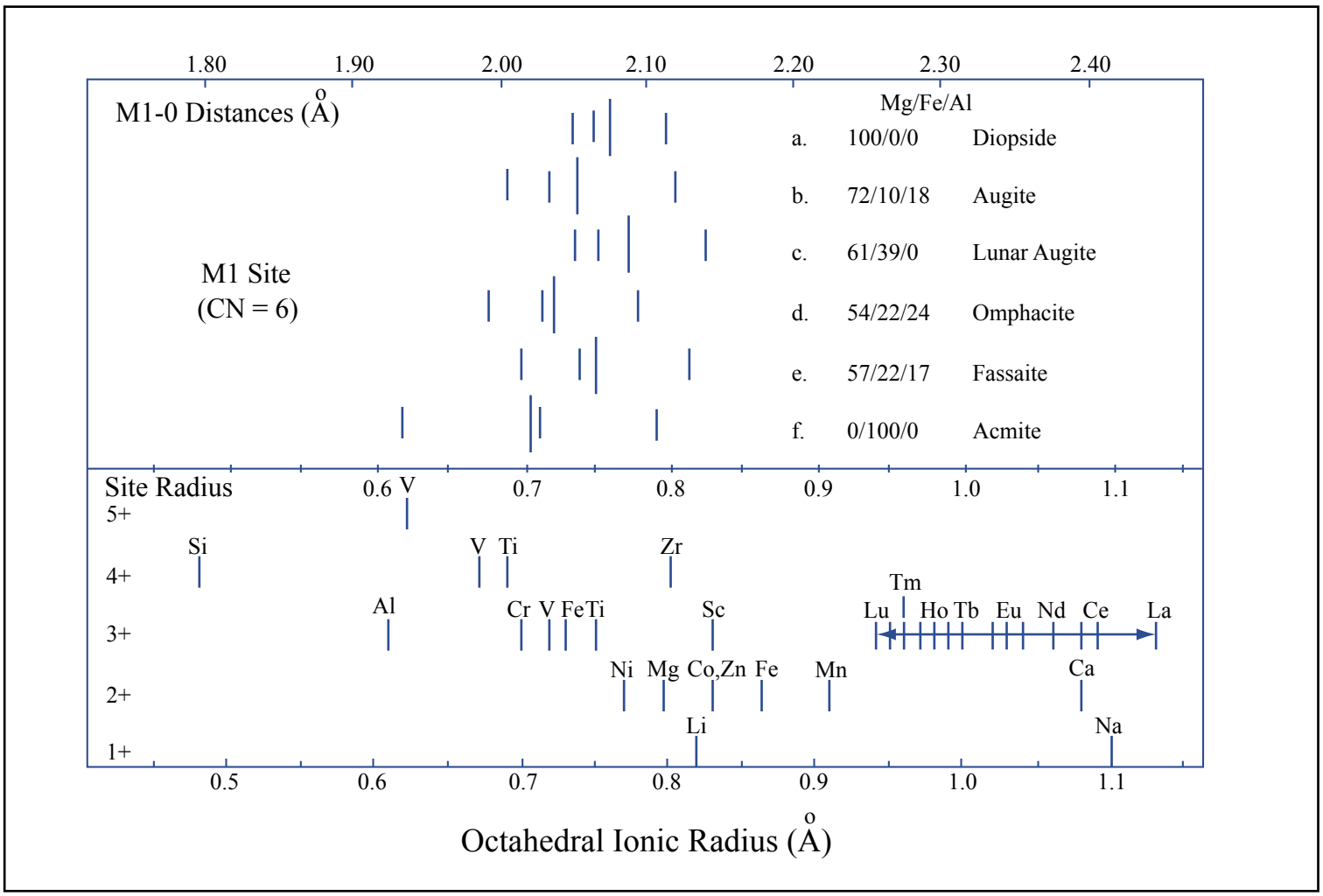

Figure by MITOpenCourseWare.

Figure 13a. Crystal chemistry of clinopyroxene. (a) upper axis shows M1-O distances measured for clinopyroxenes with different ME compositions (a through f). In this upper panel the light vertical line indicates distance (Å) for 3 pairs of M1-O bonds (Figure 12) and the bold vertical line is the average for the six M1-O bonds. The axis labeled "site radius" is the M1-O distance minus 1.32Å, the size of O-2. This site radius is an estimate of the size of the M1 site in clinopyroxene. The lower half of the panel shows ionic radii (CN 6) for several elements grouped on the basis of their commonly observed oxidation state. Ions with sizes closest to the "site radius" are predicted to be most readily incorporated into the M1 site.

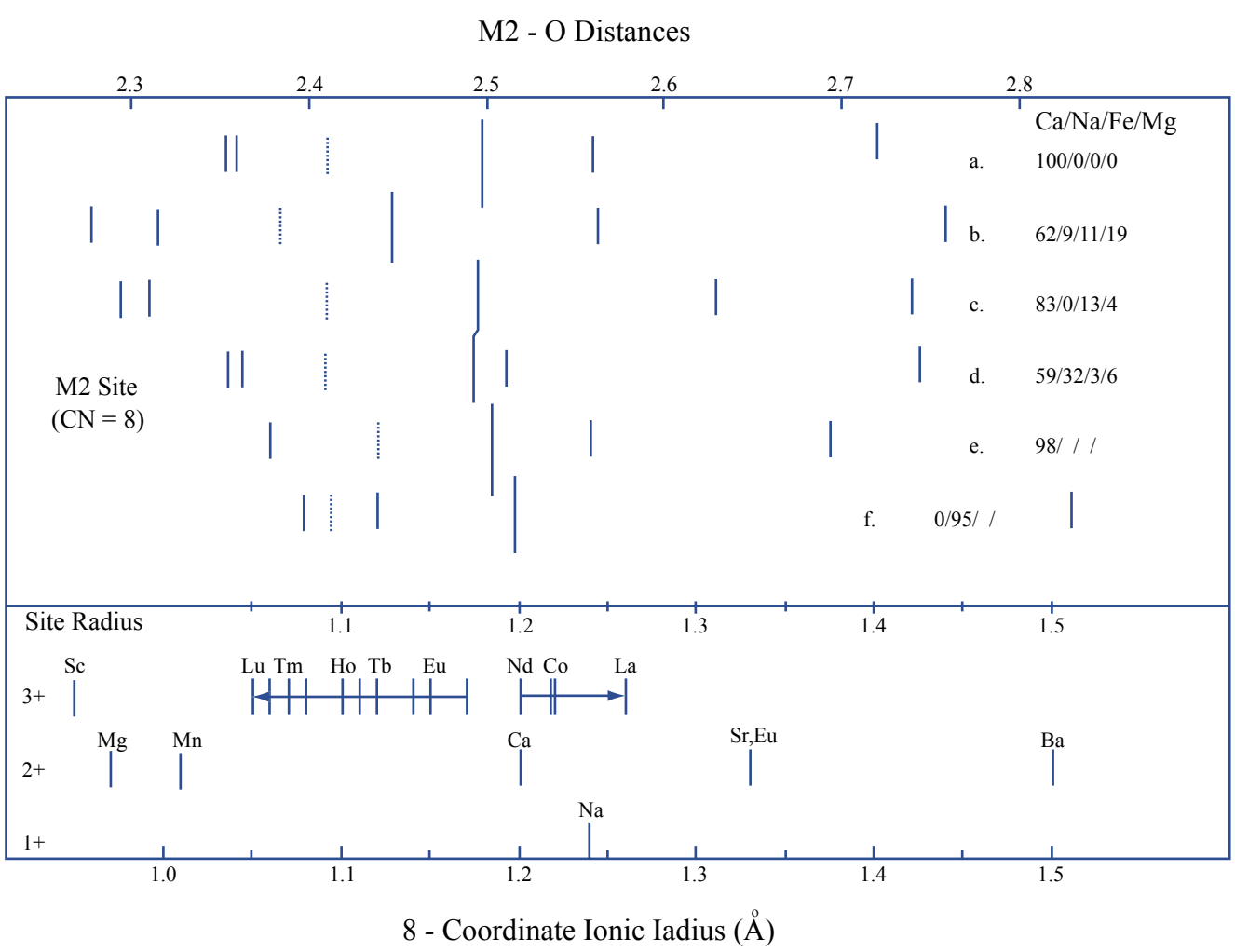

Figure by MITOpenCourseWare.

Figure 13b. The same approach as in panel a but for the M2 site. For this site there are 4 pairs of distances (Figure 12). The dashed vertical line is the average for the closest six oxygens and the bold vertical line is the average for the 8 M2-O bonds. In the lower panel ionic radii are for CN = 8. (Figure is modified from Lindstrom, 1976).

Now let's compare these predictions for REE element partitioning into clinopyroxene to measured phenocryst/matrix ratios.

Figure 14a shows that cpx phenocryst/matrix partition coefficients for REE are convex upwards with maximum values at intermediate atomic number (e.g., Sm, Eu, Gd, Tb, and Dy). The inference is that light REE (LREE), such as La and Ce, are too large and the heavy REE (HREE), such as Yb and Lu are too small compared to the ideal size of the structural M2 site in clinopyroxene (Figure 13b). Although the relative patterns for cpx/matrix are sub-parallel, there is a considerable range from ~0.1 to 1 for HREE; this wide range requires explanation (to be discussed later).

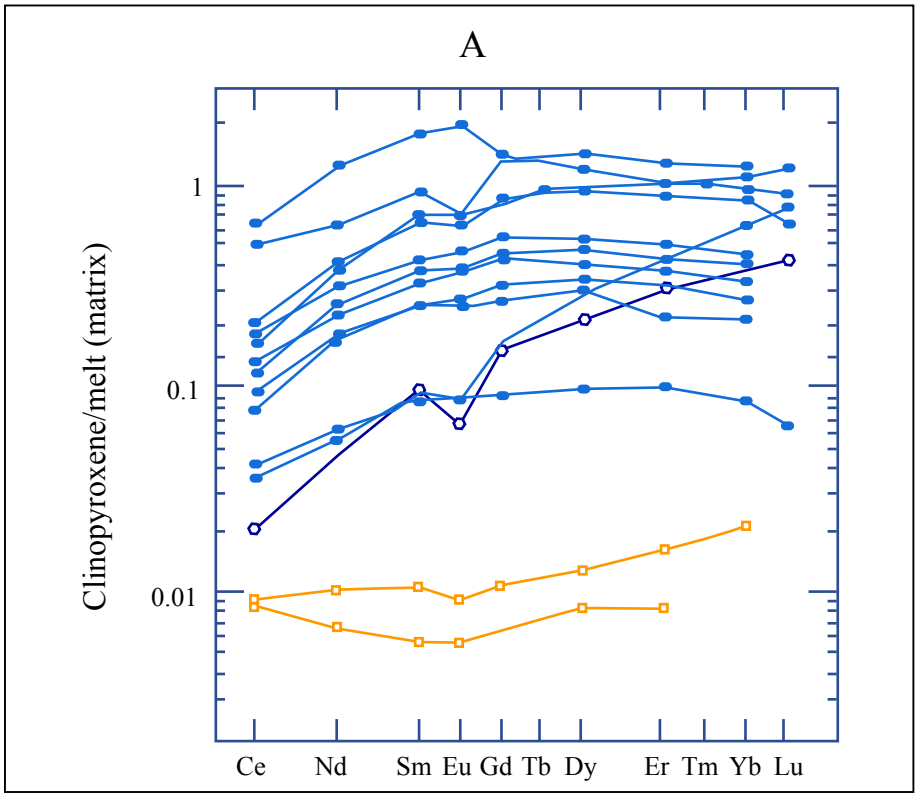

Figure 14. (Clinopyroxene phenocryst)/matrix estimates of REE partition coefficients; filled circles indicate CaO-rich clinopyroxene and open circle indicates data for a CaO-poor pyroxene, known as pigeonite.
Also shown are data for (olivine/phenocryst)/matrix estimates of REE partition coefficients (open squares). Figure adapted from Schnetzler and Philpotts (1970).

2. Olivine

Figure 14a also shows data for two sets of olivine phenocryst/matrix data and as expected the $D_{LREE}^{ol/matrix}$ are less than $D_{HREE}^{cpx/matrix}$. However, the shallow slope for olivine is surprising. This is an example of impure separates resulting from the difficulty in obtaining an olivine separate completely free of groundmass. Note that an experimental study of olivine/melt using an electron probe for controlled spatial analysis finds $D_{LREE}^{ol/melt}$ lower by a factor of 100 (Figure 14b).

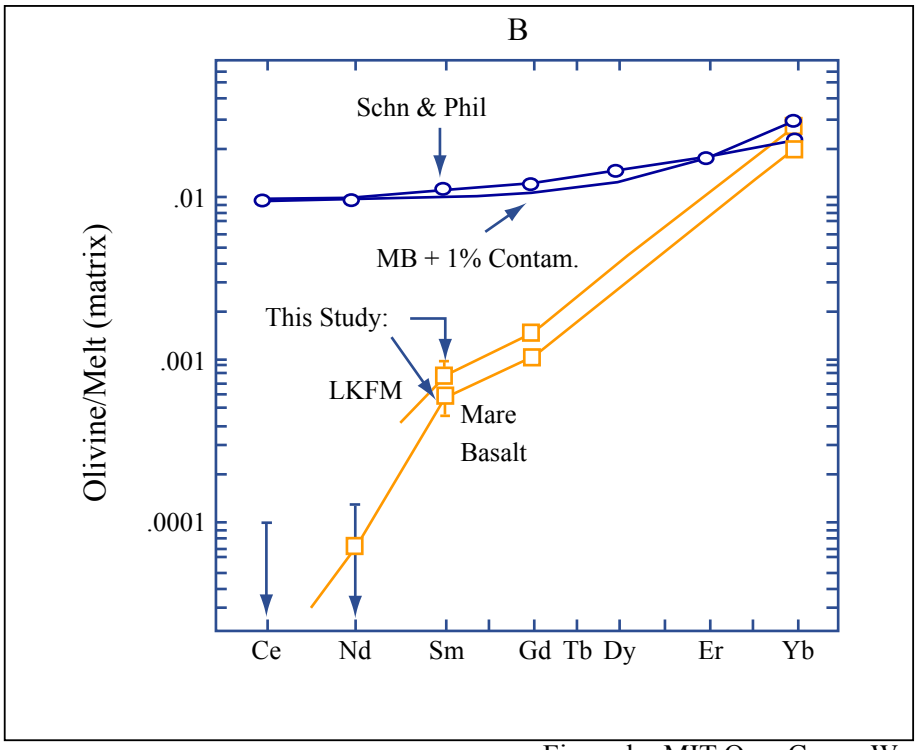

Figure by MIT OpenCourseWare.

Figure 14b. Estimates of olivine/melt partition coefficients for REE. The upper line designated by filled triangles and labeled "SCHN & PHIL" is a olivine/phenocryst pair from Figure 14a. The lower lines are for an experimental study with REE added (doped) to the system so that a electron microprobe could obtain in situ REE contents in olivine and co-existing melt (two lunar basalt compositions: LKFM and MARE basalt). The downward pointing arrows for Ce and Nd indicate upper limits because Ce and Nd abundances in olivine were below the detection of the electron microprobe. Most important is that addition of 1% mare basalt (MB) to the pure olivine closely approximates the measured olivine phenocryst/matrix DREE reported by Schnetzler and Philpotts (1970). These values are erroneous because the olivine separates were not pure. Note the contamination effects are more severe with decreasing atomic number and increasing ionic radii; i.e. as the incompatibility of REE in olivine increases. Figure adopted from McKay (1986).

3. Feldspar

Feldspar is the most abundant mineral in the earth's crust. Because it has distinctive selectivity for some trace elements such as Sr and Eu, we will find that trace element geochemistry is very useful in evaluating the role of feldspar in petrogenetic processes.

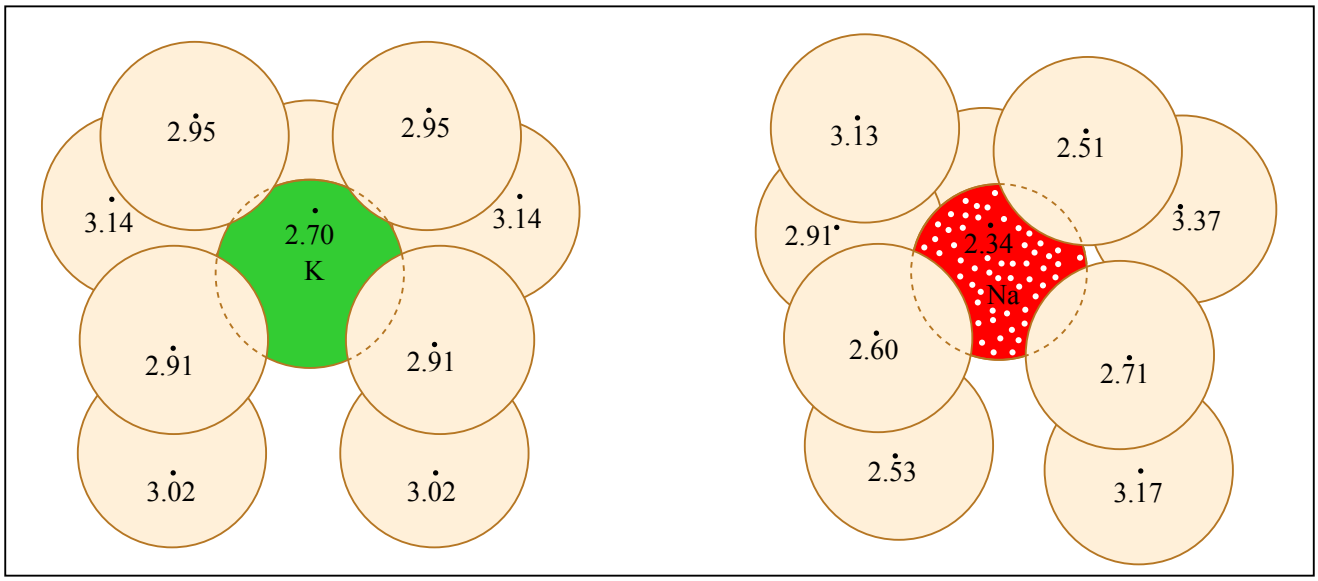

Figure by MITOpenCourseWare.

Figure 15. Oxygen coordination (CN=9) around K+1 in sanidine (left) and Na+1 in albite (right). Numbers indicate K-O and Na-O distances in angstroms (10-8 cm). Figure adapted from Figure 10 of Ribbe, 1983.

A general composition for feldspar is MT_4O_8 where T indicates ions in tetrahedral coordination with O^{-2} and M is a relatively large cation, such as Na^{+1}, K^{+1}, or Ca^{+2}. Typically the T ions are Al or Si with 1Al + 3Si plus monovalent M^{+1}, e.g., $NaAlSi_3O_8$ (albite) or $KAlSi_3O_8$ (sandine) or 2Al + 2Si with divalent M^{+2}, e.g., $CaAl_2Si_2O_8$ (anorthite). Albite and anorthite form well the known solid solution, plagioclase feldspar.

The structure is formed by all tetrahedra sharing corners in a continuous 3D framework with M cations in the cavities. For consideration of trace element partitioning into feldspar, the important characteristics are the cation-oxygen distances of 2.5 to 3.0A˚. Subtracting 1.32A˚, the size of the oxygen anion, indicates that the structural site has a size of 1.2 to 1.8A˚, i.e. much larger than the M_2 site which hosts Ca in clinopyroxene. Comparing the structural site size of 1.2 to 1.8 A˚ with cation ionic radius shows that for CN=9 the following ions have appropriate size:

K^{+1}	1.63	
Na^{+1}	1.40	
Ca^{+2}	1.26	
Sr^{+2}	1.33	
Ba^{+2}	1.55	
Eu^{+2}	1.33	but Eu^{+3} 1.15

Consistent with the idea of an ideal size for a structural site, the +3 REE ions for La (1.28A˚) to Lu (1.05A˚) are incompatible in feldspar (Figure 16) because they are much smaller than the size of the M site that is dominantly filled by Na, K, or Ca. However, feldspar/melt partition coefficients for the relatively large LREE are greater than those for the relatively smaller HREE (Figure 16); this result contrasts with the solid/melt partition coefficients for clinpyroxene and olivine (Figure 14). A distinctive feature of feldspar is that if both Eu^{+2} and Eu^{+3} exist, the larger Eu^{+2} is preferred by feldspar. In fact, feldspars are characterized by a relative enrichment in Eu, described as a positive Eu anomaly (Figure 16). Hence relative enrichment of Eu is a characteristic of feldspar and this observation was pivotal in understanding the origin of lunar highland rocks and maria basalt (Taylor, 1975).

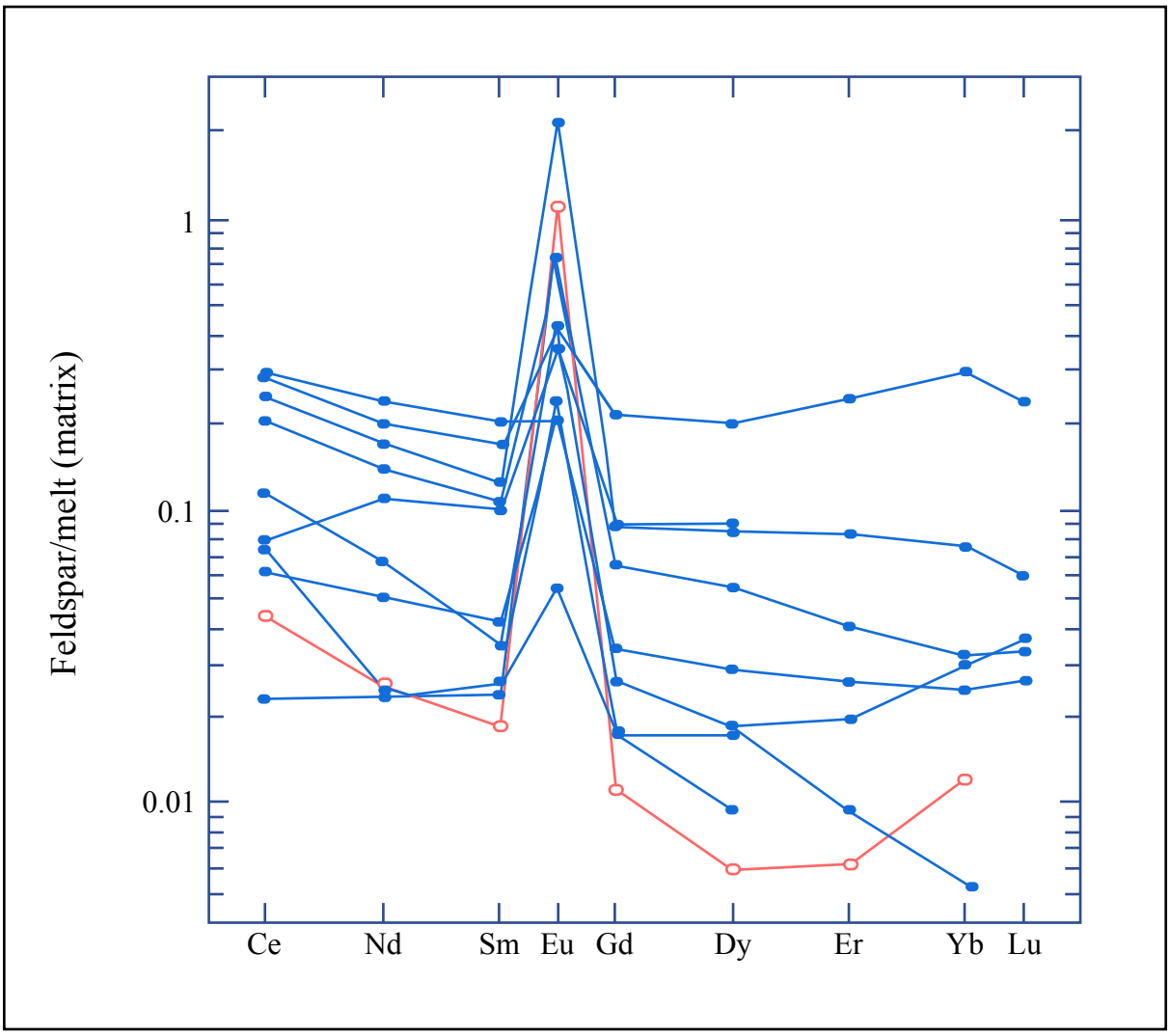

Figure 16. REE partition coefficients for (plagioclase phenocryst)/matrix (solid circles) and (K-feldspar phenocryst)/matrix (open circles). Note the overall negative slope, the range in absolute values and the peak at Eu, known as the Eu anomaly. This anomaly is a result of preferential incorporation of Eu+2 into feldspar. Figure from Schnetzler and Philpotts, 1970.

Measured plagioclase phenocryst/matrix data show that Sr is compatible in feldspar, and is increasingly compatible as An/Ab ratio decreases (Figure 17). Hence Sr, like Eu, is an indicator for plagioclase but interestingly not for the Ca-rich mineral clinopyroxene where Sr is incompatible even in the relatively large M2 site (Figure 17).

The large ions Rb^{+1} and Ba^{+2} are incompatible in plagioclase but they are compatible in micas which has a suitable structural site for large cations; e.g., phlogopite is $KMg_3(AlSi_3O_{10})(OH)_2$; clearly it can incorporate large ions such as K, and small ions such as Mg^{+2} but it is probably not a good host for ions with ionic radii of 1 to 1.2 A˚. Indeed REE are found to be incompatible in mica (e.g., Foley et al., 1996).

Mineral	An	D_{Sr}	D_{Ba}	D_{Rb}
Plagioclase				
GSFC 240	96.7	1.27	0.05	0.05
GSFC 233	92.8	1.31	0.14	0.07
GSFC 204	87.3	1.66	0.24	0.19
GSFC 184	80.3	1.66	0.13	0.04
HHP-66-19	78.8	1.77	0.26	0.06
GSFC 271	77.1	1.83	0.20	0.05
GSFC 208	65.2	1.26	0.15	0.03
GSFC 218	51.4	2.84	0.36	0.05
GSFC 225	45.8	2.75	0.59	0.14
K-feldspar				
GSFC 266		3.87	6.12	0.66
Clinopyroxene				
GSFC 25		0.43	0.36	0.28
GSFC 204		0.09	0.03	0.04
Mica				
SFC 193		0.08	1.09	3.06
GSFC 218		0.12	6.36	3.26
GSFC 266		0.07	15.3	0.94

Figure 17. Phenocryst/matrix partition coefficients for Sr, Ba and Rb. Note that Sr is compatible in plagioclase and that D_{Sr} increases with decreasing An content. In contrast Sr, Ba and Rb are incompatible in clinopyroxene and Ba and Rb are compatible in mica. Data from Philpotts and Schnetzler, 1970.

4. Garnet

In a basaltic system, at low pressure, e.g., 1 bar, plagioclase, feldspar is the aluminous (Al -rich) phase but as pressure increases to correspond to upper mantle pressures, garnet replaces plagioclase feldspar as the stable aluminous phase. Consequently, the partitioning of elements into garnet is relevant when evaluating the formation of basaltic magma as a partial melt of upper mantle rocks, e.g, garnet peridotite and eclogite. Garnet is not found as phenocrysts in basaltic rocks; therefore garnet phenocryst/basaltic matrix data are not available. However, garnet occurs in upper mantle rocks found as xenoliths (garnet lherzolites and eclogites), and it is possible to measure cpx/garnet partition coefficients (e.g., Harte and Kirkley, 1997; Shimizu, 1975).

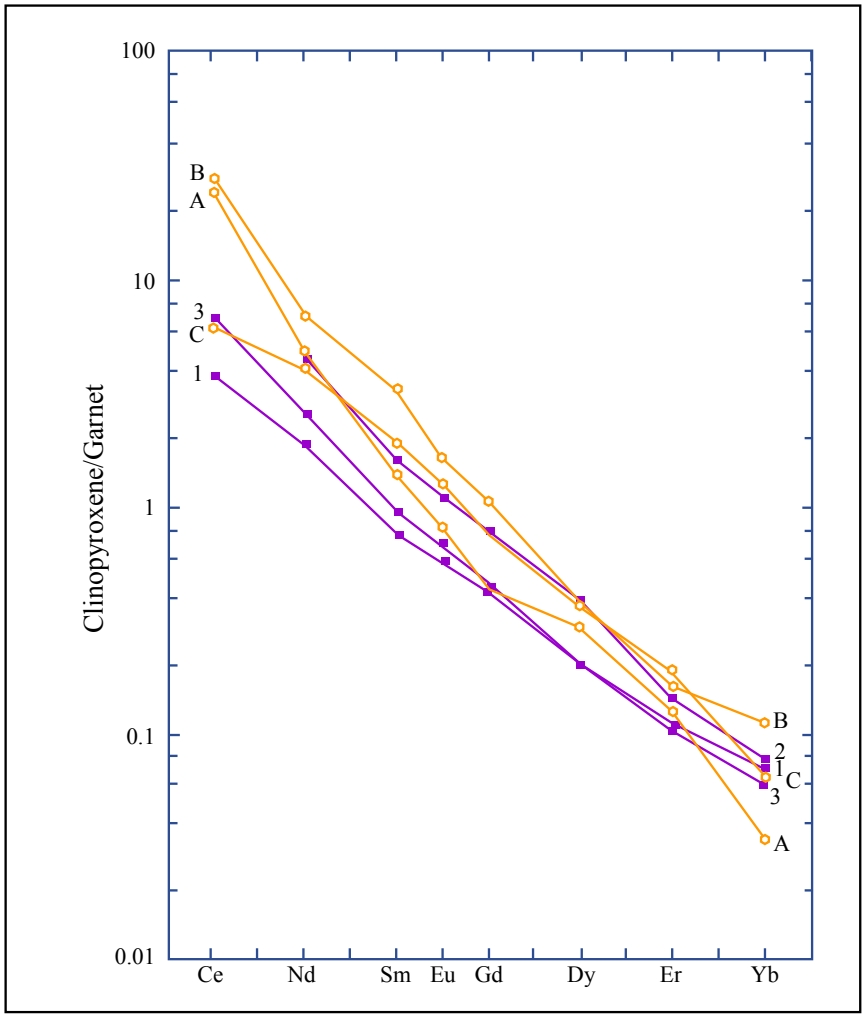

Figure 18. REE partitioning between coexisting clinpyroxene and garnet in garnet lherzolites (from Shimizu, 1975).

Figure 18 shows that $D_{cpx/garnet}$ increases steeply from the HREE to LREE.

Consider that

$$D_{gt/melt} = \frac{\text{conc gt}}{\text{conc melt}} = \frac{\text{conc cpx}/\text{conc melt}}{\text{conc cpx}/\text{conc gt}} = \frac{D_{cpx/melt}}{D_{cpx/gt}}$$

With the measured $D_{cpx/gt}$ for a garnet lherzolite and an assumed $D_{cpx/melt}$, Shimizu (1975) determined the following values for garnet/melt partition coefficients.

D = garnet/melt

Ce	0.01
Nd	0.04
Sm	0.16
Fe	0.26
Gd	0.40
Dy	0.95
Er	1.6
Yb	3.0

The significant result is the HREE, such as Yb are compatible in garnet. Analogous to Ni for olivine and Sc for clinopyroxene HREE abundances are very sensitive to a petrogenetic role for garnet.

As with clinopyroxene, the crystal chemistry of garnet is useful for understanding why garnet strongly prefers the smaller HREE ions. The general formula for garnet is $X_3^{+2}Y_2^{+3}Z_3^{+4}\ O_{12}$. The structure is composed of a framework of ZO_4^{-4} tetrahedral and YO^6 octahedra which share corners to form 8 coordinated dodecahedral (distorted cube) XO_8 sites. It is this CN = 8 site that has a site radius similar to the HREE; hence they are compatible.

F. Effect of melt composition on partitioning of REE

We have focused on the importance of crystal structure in controlling mineral/melt partition coefficients and ignored melt structure, implicitly assuming that melts do not discriminate between ions of different radii and charge as strongly as minerals. However, melt structure does vary considerably from the extremes of basalt to rhyolite. The effects of melt composition are more directly evaluated in experimental studies (to be discussed in Lecture 7). Nevertheless, early comparisons of phenocryst/basaltic matrix and phenocryst/dacitic matrix showed that melt composition is also important in partitioning; most elements become more compatible as the melt increases in SiO_2 content (Figure 19).

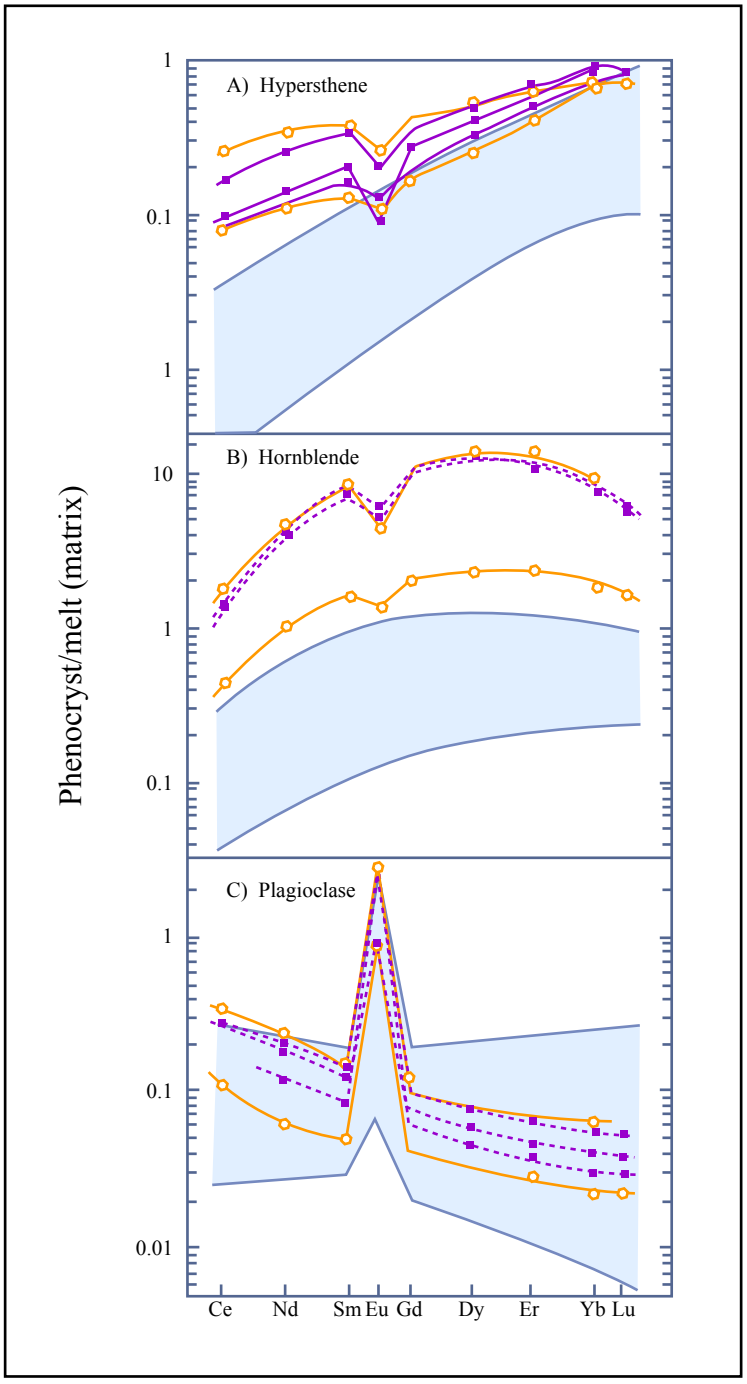

Figure by MITOpenCourseWare.

Figure 19. Data points indicate phenocryst/dacitic matrix partition coefficients; shaded fields indicate range for basaltic and andesitic matrices. No difference is observed for plagioclase but hypersthene (orthopyroxene) and amphibole partition coefficients are notably larger for the dacitic matrix. As an aside, REE partition coefficients for amphibole (hornblende) are similar to those for clinopyroxene in both a relative and absolute sense (compare with Figure 14c). The figure is from Nagasawa and Schnetzler (1971).